Planar Laser-Induced Fluorescence in a Turbulent Premixed Flame to analyze Large Eddy Simulation Models

R.Knikker, D.Veynante, J.C.Rolon and C.Meneveau†

Laboratoire EM2C, Ecole Centrale Paris and CNRS
Châtenay-Malabry Cedex, France.

† Permanent address: Mechanical Engineering
Johns Hopkins University, Baltimore, MD USA.

ABSTRACT

Large eddy simulations (LES), where the large-scale motions are explicitly computed, is a promising tool for numerical simulations of reactive flows which generally exhibit large coherent structures. Nevertheless, subgrid-scale models have to be developed to describe the effects of the smaller flow motions not resolved in the simulation. An experimental method is presented for validation and development of these models, based on OH-LIF imaging in a V-shaped turbulent premixed flame stabilized behind a triangular flame holder. Instantaneous flame fronts are obtained by separating fresh and hot gases (figure 1a). A subgrid-scale combustion model is investigated here using the filtered progress variable approach. The curvature of the resolved flame front (figure 1b) appears to provide a promising estimation of the unresolved flame surface density.

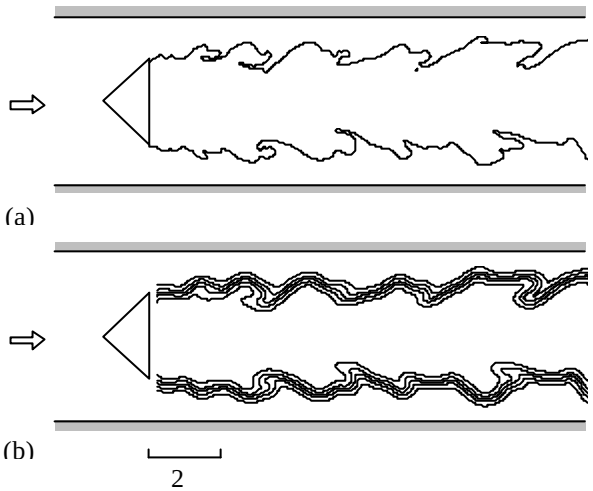

Figure 1. Visualization of the instantaneous flame front of a premixed turbulent propane/air flame stabilized behind a triangular flame holder (a) (mean inlet velocity <v>=10 m/s, equivalence ratio j=0.8) and

INTRODUCTION

Large eddy simulations (LES), where the large scale motions are explicitly computed, is a promising tool for numerical simulations of reactive flows. This approach seems particularly suited for combustion instabilities, which generally exhibit large coherent structures. Nevertheless, a difficulty is encountered since the flame front thickness of a premixed flame is in the order of 1 mm and is generally much smaller than the numerical grid size. Temperature and mass fractions are therefore very stiff variables and cannot be resolved on the computational grid. To overcome this difficulty, several approaches have been proposed.

The flame tracking technique or G-equation (Kerstein *et al*. 1988; Bourlioux *et al*. 1996; Menon 1996) makes use of a field variable G. The flame is viewed as an infinitely thin propagating surface, defined by the iso-level $G=G^*$. The variable G can be smoothed out to be resolved on the numerical grid. An approach closely related to the G-equation is the filtered progress variable c. In this case the chemical reaction mechanism is reduced to one equation, which is then filtered with a filter size greater than the grid size (Boger *et al*. 1998). An advantage of this method is that the definition of the variable c can be based on a physical parameter and can, therefore, more easily be compared with experimental data. A third approach is to simulate an artificially thickened flame (Butler *et al*. 1977; Angelberger *et al*. 1998; Colin *et al*. 2000).

Large eddy simulation of turbulent combustion requires the development of the so-called subgrid-scale models, which account for the small-scale effects not resolved in the simulation. In the context of the filtered progress variable approach, the model should represent the small-scale structures (wrinkles) of the flame that are lost by the filtering process. The flame surface appears as a important parameter, directly related to the reaction rate. Visualization of the instantaneous flame surface is possible with planar laser-induced fluorescence (LIF). This technique is, therefore, a powerful tool for the validation and development of subgrid-scale models and is used in this paper to analyze a turbulent premixed flame stabilized on a triangular-shaped obstacle.

THEORY

In the classical theory of premixed flames, assuming identical mass and thermal diffusivities, the reactive species mass fractions and the temperature are all linearly related and may be expressed in terms of a reaction progress variable c (c=0 in fresh gases and c=1 in burned gases), following the balance equation:

$$\frac{\partial \rho c}{\partial t} + \nabla \cdot (\rho \mathbf{u} c) = \nabla \cdot (\rho D \nabla c) + \dot{\omega} = \rho w |\nabla c| \qquad (2)$$

where D is the diffusion coefficient, $\dot{\omega}$ the reaction rate and w the displacement speed of the iso-c surface relative to the flow field (as in the G-equation formulation by Kerstein *et al*. (1998)) . In LES, the balance equation (2) is spatially filtered. The filtering operation is defined as:

$$\overline{Q}(\mathbf{x}, t) = \int Q(\mathbf{x}', t) F(\mathbf{x} - \mathbf{x}') d\mathbf{x} \qquad (3)$$

where $\overline{Q}$ denotes a filtered quantity and F is a spatially homogeneous filter function. In our analysis, a Gaussian-shaped spatial filter is used:

$$F(\mathbf{x}) = \left(\frac{6}{\pi \Delta^2} \right)^{3/2} \exp\left(-\frac{6}{\Delta^2} |\mathbf{x}|^2 \right) \qquad (4)$$

The filter size Δ is chosen large enough so that the filtered fields may be resolved on the numerical grid.

Applying this filter to the c balance equation gives:

$$\frac{\partial \overline{\rho}\widetilde{c}}{\partial t} + \nabla \cdot (\overline{\rho}\widetilde{\mathbf{u}}\widetilde{c}) + \nabla \cdot [\overline{\rho}(\widetilde{\mathbf{u}c} - \widetilde{\mathbf{u}}\widetilde{c})] = \nabla \cdot (\overline{\rho D \nabla c}) + \overline{\dot{\omega}} = \overline{\rho w |\nabla c|} \qquad (5)$$

where $\widetilde{Q} = \overline{\rho Q}/\overline{\rho}$ denotes a mass weighted filtered quantity. This equation contains several terms that need to be modeled. Our attention is focussed here on the last RHS term denoting the spatially filtered flame front displacement. This term may be rewritten as (Piana *et al*., 1997):

$$\overline{\rho w |\nabla c|} = <\rho w>_S \Sigma = <\rho w>_S \Xi |\nabla \overline{c}| \qquad (6)$$

where the filtered flame front displacement is expressed in terms of the subgrid-scale flame surface density $\Sigma = \overline{|\nabla c|}$ or the flame wrinkling factor Ξ. The term $<\rho w>_S$ denotes the subgrid-scale surface-averaged mass-weighted displacement speed. Assuming a thin wrinkled flame, where turbulence wrinkles the flame but does not affect its inner structure, $<\rho w>_S$ may be estimated from the laminar flame speed S_L and the fresh gas density ρ_u as $<\rho w>_S = \rho_u S_L$.

According to equation (6), the flame surface density may be decomposed into a resolved and an unresolved contribution:

$$\Sigma = \Xi |\nabla \overline{c}| = \underbrace{|\nabla \overline{c}|}_{\text{(resolved part)}} + \underbrace{(\Xi - 1)|\nabla \overline{c}|}_{\text{(unresolved part)}} \qquad (7)$$

where the unresolved contribution has to be modeled.

EXPERIMENTAL SETUP

A schematic diagram of the experimental configuration is shown in figure 2. A mixture of propane/air is injected at ambient conditions through a long duct into a rectangular burner chamber. The upper and lower burner walls are made of a ceramic material for thermal isolation and the lateral walls are transparent artificial quartz windows allowing optical access to the entire flame. The height, depth and length of the chamber are 50, 80 and 320 mm, respectively. The air and propane flows are set using calibrated mass flow controllers (Bronkhorst Hi-Tec). The maximum mean inlet velocity is 25 m/s corresponding to a mass flow of 120 g/s and a Reynolds number of 41.700. Hot-wire measurements revealed turbulent intensities of about 5 % at the inlet. A stainless steel triangular flame holder (height 25 mm) is placed in the burner chamber, providing a blockage ratio of 50 %. A V-shaped turbulent flame is stabilized by hot gases recirculating behind the flame holder.

Qualitative OH concentration measurements are obtained using planar laser-induced fluorescence. A Nd:YAG laser (Continuum Powerlite 7000), operating at 10 pulses per second with a typical duration of 7 ns, is frequency-doubled to pump a dye-laser (Continuum ND62) operating on Rhodamine 590. The dye-laser beam is then passed through a KDP frequency doubling crystal and transformed into a laser sheet using cylindrical lenses. The laser frequency is tuned to the isolated $Q_1(5)$ line in the $A^2\Sigma^+(v'=1) \leftarrow X^2\Pi(v''=0)$ band of OH at 282.667 nm. The laser sheet (typical pulse energy 12 mJ) is introduced into the burner chamber by two narrow artificial quartz windows embedded in the ceramic walls. The resulting fluorescence is visualized by a 512x512 pixel CCD camera, coupled to a gated intensifier (Princeton Instruments). Two filters (WG305 and 03FIM024) are placed in front of the camera to collect only the broadband radiation around 310nm of the vibrational (0,0) and (1,1) band of OH. A pulse/delay generator DG535 (Stanford Research Systems Inc.) is used to synchronize camera and laser system and to set the exposure time to 100ns. Images cover up to 12 cm downstream of the flame holder with a spatial resolution of 0.25 mm/pixel. No attempts are made to calibrate the OH concentration measurements.

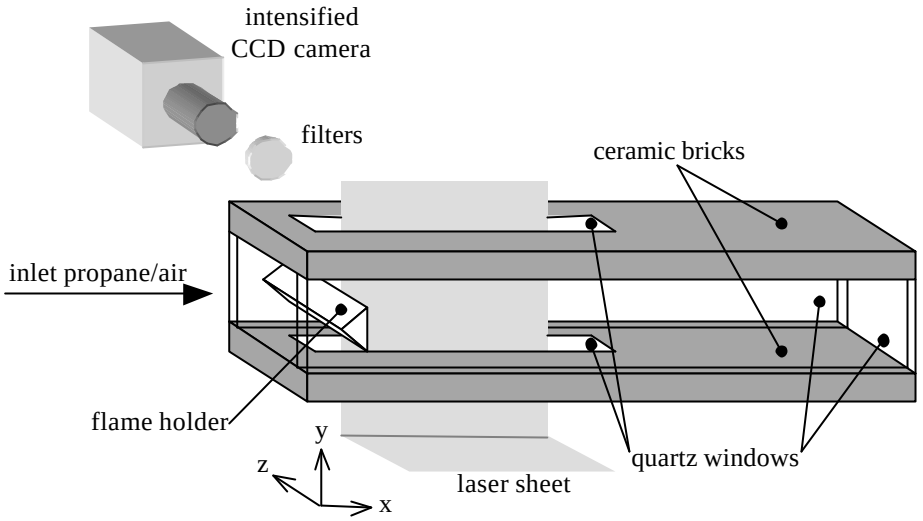

Figure 2. Experimental configuration. A propane/air mixture is injected into the combustion chamber and a turbulent flame is stabilized behind a triangular-shaped obstacle. LIF images are obtained by passing a laser sheet through two narrow windows and visualizing the resulting radiation with an intensified CCD camera.

A typical LIF image is displayed in figure 3a. Burned gases are characterized by the presence of OH radicals (visible as dark regions in the images). High concentration gradients are observed within the reaction zone. Signal levels in fresh gases are almost zero due to subtraction of background images, obtained by temporarily blocking the laser light. Preprocessing of the images include a 3x3 median filter and a correction for spatial variations of the laser intensity along the horizontal axis. An intensity profile, defined as the mean LIF signal on the centerline (y=0) of the burner, is used to egalize signal levels in the burned gas regions of instantaneous images.

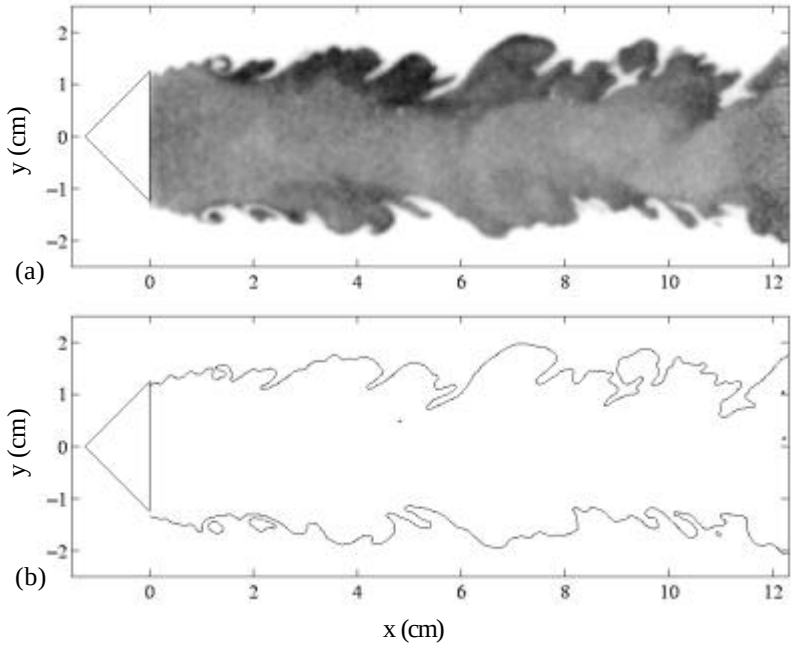

Figure 3. Instantaneous LIF image of the OH radical in a turbulent premixed propane/air flame stabilized on a triangular-shaped obstacle (<v>=20 m/s and j=1.0) (a) and the extracted flame front (b).

Assuming an infinitely thin flame front, fresh gases (c=0) can be separated from hot gases (c=1) by applying a threshold. However, the OH concentration within the burned gases show large spatial variations and a single threshold level is difficult to define. A low threshold level generally implies a loss of details, whereas high levels result in the appearance of holes in the burned gas. Therefore, another method has been developed, especially adapted to this problem. As a first step, flame fronts are detected using spatial gradients of the LIF signal. Regions close to the flame front generally exhibit large OH concentrations. Therefore, the threshold (applied to the original image) is locally increased to reveal the details of the flame front. On the other hand, the threshold level in regions far from the reaction zone is kept sufficiently low to avoid the appearance of holes. The obtained threshold level field is now subtracted from the LIF image and the final flame front is defined as the zero value iso-contour. The result is shown in figure 3c.

RESULTS

Flame characteristics

A large database has been developed under various operating conditions. Figure 4 illustrates the effect of changing the inlet velocity and the equivalence ratio on flame characteristics. Nearly stoichiometric flames at small Reynolds numbers show only slightly wrinkled flame fronts. Increasing the inlet velocity or decreasing the equivalence ratio results in a more wrinkled flame front and the formation of fresh and hot gas pockets. This finding is probably due to an increase of the ratio u'/S_L, comparing turbulent intensity to the propagation velocity of the flame surface. Unfortunately, velocity fluctuations measurements are not yet available and this hypothesis cannot be verified.

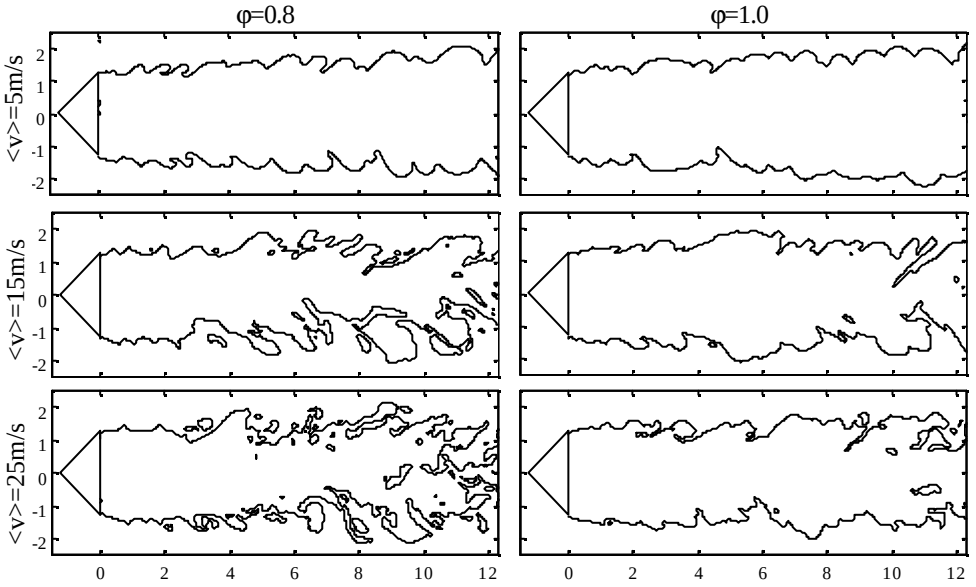

Figure 4. Instantaneous flame fronts extracted from OH-LIF images at various operating conditions. Mean velocity and equivalence ratio of the propane/air mixture at the inlet are indicated.

The small-scale structures that appear at high Reynolds numbers suggest the presents of three-dimensional effects. In order to investigate this point, additional transverse images are obtained. The laser sheet is now oriented perpendicular to the downstream direction and introduced into the combustion chamber via the lateral windows. The intensified CCD camera is placed facing the laser sheet at an angle, resulting in an optical deformation of the image. A reference image of a rectangular grid is used to restore the data before flame front extraction. Typical examples are shown in figure 5.

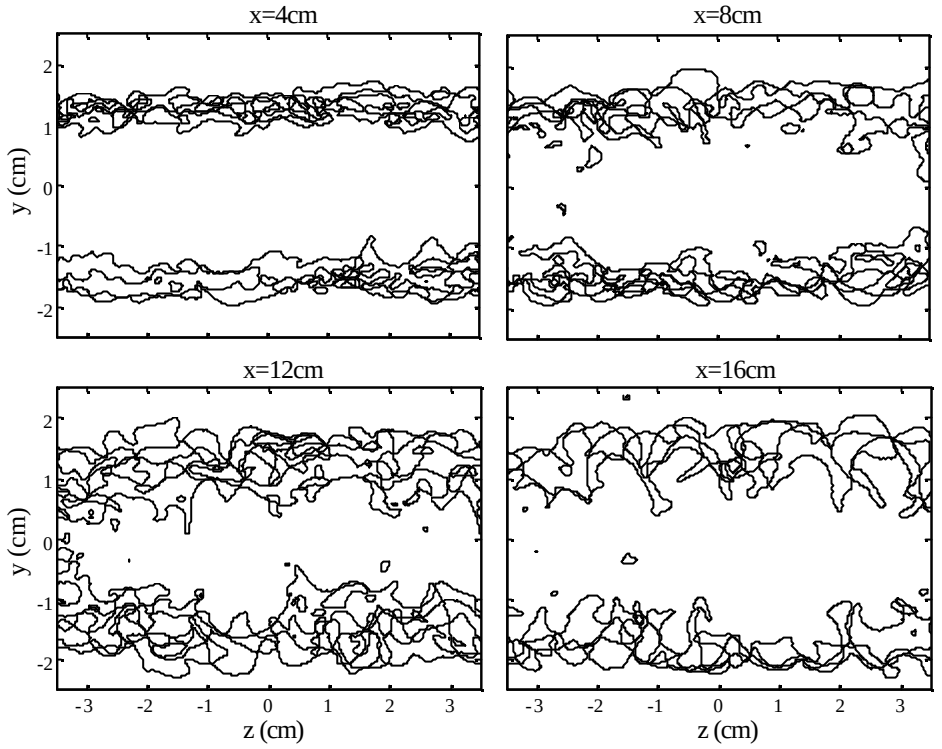

Figure 5. Instantaneous flame fronts in the plane perpendicular to the downstream direction at 4, 8, 12 and 16 cm from the flame holder for <v>=20 m/s and j=1.0 (conditions corresponding to figure 3). Each figure contains four realizations.

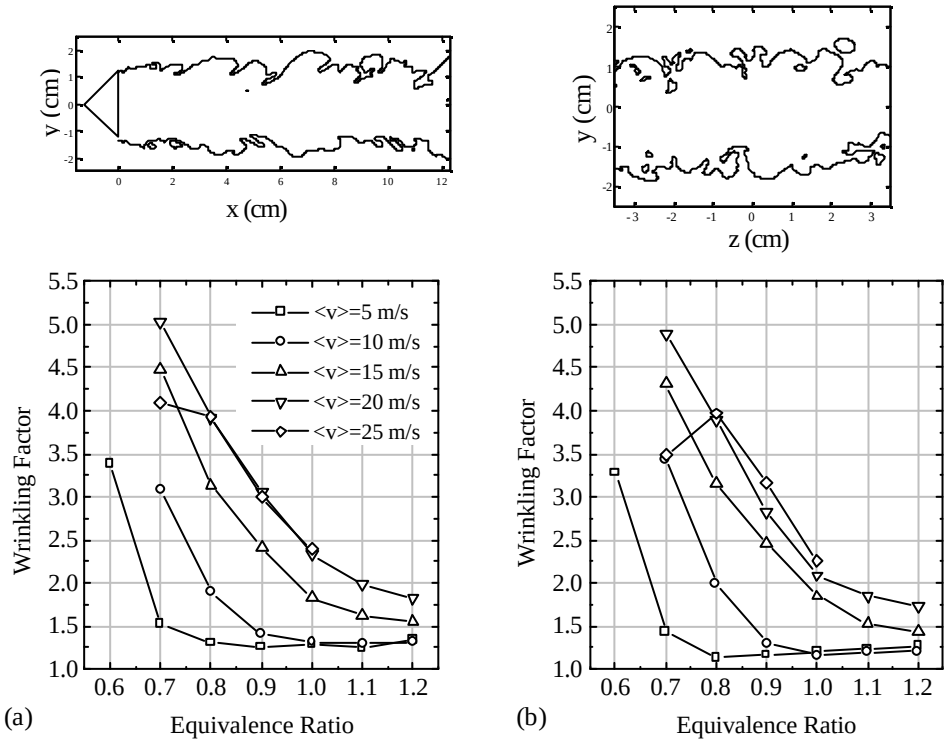

Figure 6. Flame surface wrinkling factor calculated from the downstream images (a) and the transverse images (b) at x=8 cm from the flame holder for various operating conditions. Results are calculated from areas indicated in the upper images.

The results show a highly wrinkled flame surface indicating important three-dimensional effects. Length scales of the flame front structures seem to depend on the distance from the flame holder, as observed also in the previously described downstream images. In fact, flame characteristics in both experiments are very similar. This is illustrated in figure 6 by comparing flame surface wrinkling factors, defined as the ratio of the actual flame surface area to the surface area of an unwrinkled flame. Wrinkling factors are calculated from the downstream and traverse images by integrating the frame front length over the area indicated in the figure. Regions close to the lateral walls are not used to avoid its influence on the flame characteristics. Results correspond to flow conditions at x=8 cm downstream of the flame holder. Statistical errors are minimized by averaging over 50 images. Corresponding to observations, high wrinkling factors are found for low equivalence ratios and high Reynolds numbers. However, the values found for the traverse images are in the same order of magnitude as for the downstream images. Apparently, the flame is fully three-dimensional.

Analysis of the unresolved flame surface density

The spatially filtered progress variable is displayed in figure 7a, using a filter size of Δ=5 mm. The small-scale structures present in the actual flame are lost by the filtering process and have to be modeled. These models should correctly predict the subgrid-scale flame surface density shown in figure 7b. As a first step, a decomposition of this term into a resolved and a non-resolved part is performed, according to equation 7. In the limit of an infinitely small filter size (or in the case of a flat flame) the unresolved term tends towards zero. A contribution is, therefore, only expected in the presence of small-scale structures and regions of high curvature of the filtered progress variable, as shown in figure 7c.

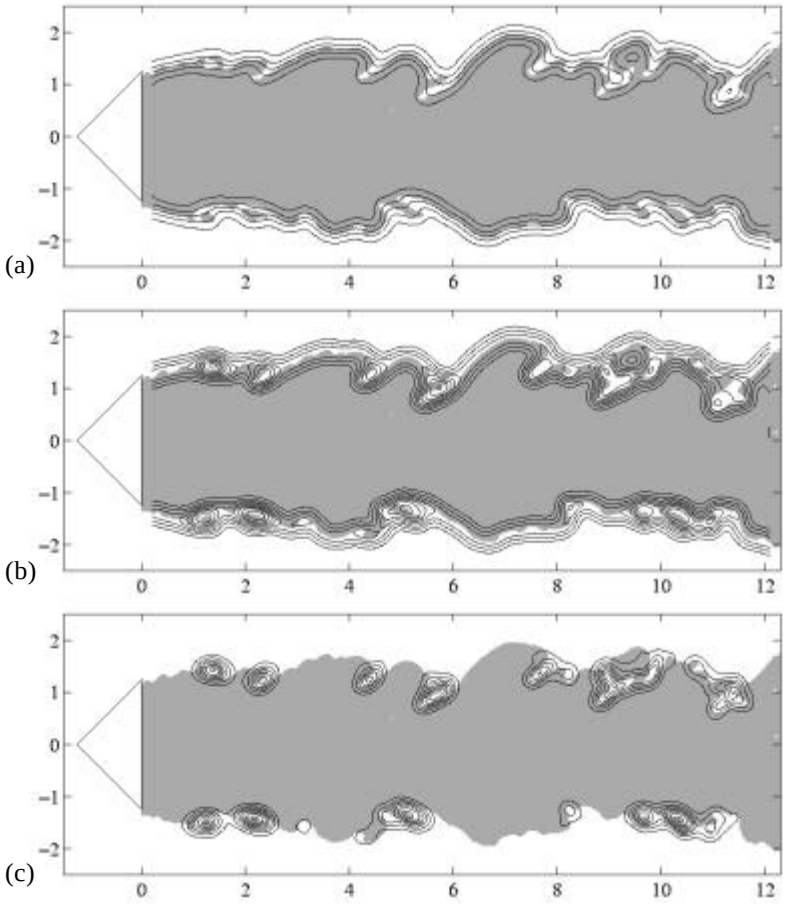

Figure 7. The filtered progress variable $\bar{c}$ (a), the flame surface density S (b) and the unresolved contribution $\Sigma - |\nabla \bar{c}|$ (c). In gray is displayed the binarised progress variable c.

Current subgrid-scale models for premixed combustion are often based on the subgrid-scale velocity fluctuations $u_{rms,\Delta}$ (specifically, on the ratio $u_{rms,\Delta}/S_L$). The G-equation, for example, uses frequently an extension of an empiric relation applied in RANS simulations:

$$\Xi = 1 + \alpha \left(\frac{u_{rms,\Delta}}{S_L} \right)^n \tag{8}$$

where α and n are model parameters. In the context of the thickened flame approach, Angelberger *et al*. (1998) and Colin *et al*. (2000) proposed a similar model introducing an efficiency function, which compares wrinkling factors of the thickened flame to that of the actual one. Recently, this approach was used by Nottin *et al*. (2000) to simulate an acoustically excited flame in the same configuration. Numerical results are compared with experimental data using the methods described in this paper. The large-scale structures observed in the experiment are also found in the simulation, but the location of maximum values of the unresolved surface density is not well predicted. Based on these results, the possibility of using the filtered progress variable to predict the unresolved term is investigated here.

A flame surface density model based on flame curvature

As shown in figure 7 and in the findings of Nottin *et al*. (2000), the unresolved flame surface density seems to be related to the curvature $\left|\nabla \cdot \mathbf{N}\right|$ of the resolved c-field. Then, the following model is proposed:

$$\Sigma - \left|\nabla \overline{c}\right| = k \overline{\left|\nabla \cdot \mathbf{N}\right| M(\overline{c})} \tag{9}$$

where k is a non-dimensional model parameter, $\mathbf{N} = \nabla \overline{c} / \left|\nabla \overline{c}\right|$ the unit vector normal to the iso-contours of the filtered progress variable and M is a masking function to avoid undesired contributions in regions far away from the flame front. In the present analysis, a simple binary function is used:

$$M(\overline{c}) = \begin{cases} 1, & \text{for } 0.1 < \overline{c} < 0.9 \\ 0, & \text{elsewhere} \end{cases} \tag{10}$$

The curvature of the filtered progress variable field $\left|\nabla \cdot \mathbf{N}\right|$ exhibits high values in regions where the resolved flame is highly curved, corresponding in general to the locations where a high contribution of the unresolved flame surface density is found (compare figure 7a and 7c). However, these high curvatures are presented as narrow regions whereas the unresolved contributions are smoothed out. Therefore, a spatial filter similar to that used for filtering the progress variable is applied. Note that $\left|\nabla \cdot \mathbf{N}\right|$ scales with the filter size Δ (the larger Δ is, the lower is the resolved curvature).

This model is now analyzed using high-resolution images (0.13 mm/pixels). Results are averaged over 50 shots and regions close to boundaries are not used. Figure 8a shows the correlation coefficient of the unresolved flame surface density and the proposed model. In almost all of the cases the correlation coefficient is higher than 80%. Figure 8b shows an estimation of the model parameter k using the minimum least-squares method. Apparently, the results are relatively independent of the equivalence ratio despite the changes in the flame characteristics. This suggest that the parameter k depends mainly on the Reynolds number rather than chemistry (note that chemistry is still included in the simulation through the displacement speed $<\rho w>_S$).

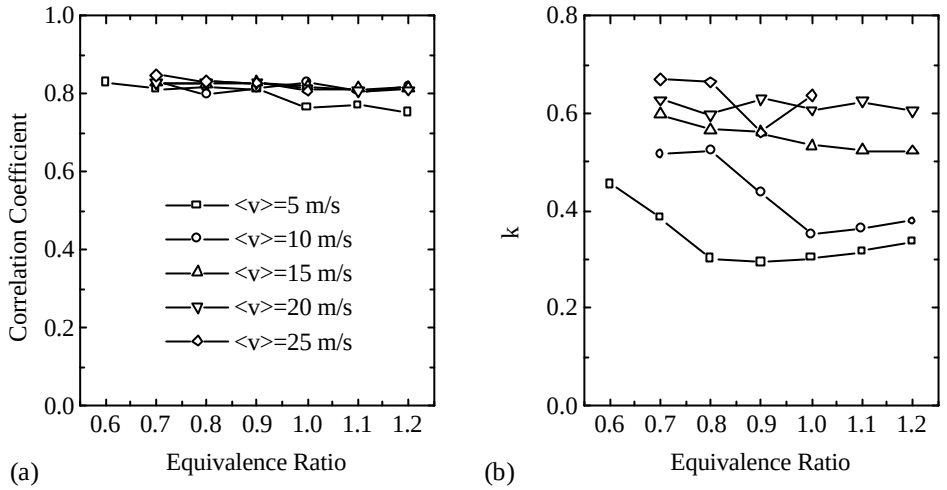

Figure 8. The correlation between the unresolved flame surface density and the proposed model (a) and the estimation of the model parameter k using the least-squares method (b).

The influence of the filter size on the results is displayed by figure 9. The model parameter k depends almost linearly on the filter size. In terms of dimensionless parameters, k may depend on Δ/δ_c, where δ_c is a cutoff length-scale (e.g. the laminar flame thickness), and also on $u_{rms,\Delta}/S_L$. For large filter sizes, the correlation coefficient decreases gradually. This can be explained by the fact that the flame structures, much smaller than the filter size, do not influence the resolved flame and, therefore, are not represented by the model. The results show that the best agreement (highest correlation) is observed when the filter size is of the same order of magnitude as the flame structures that need to be modeled.

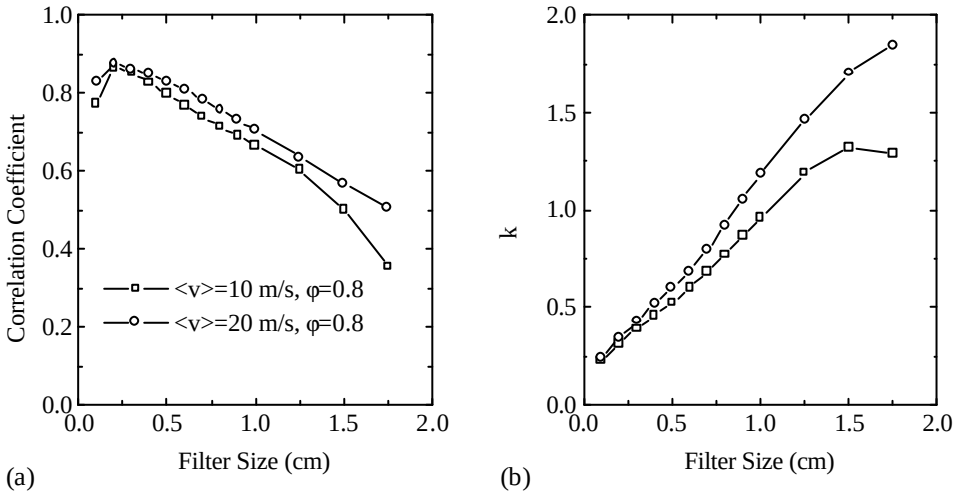

Figure 9. The influence of the filter size on the correlation between the unresolved flame surface density and the proposed model (a) and on the model parameter k (b).

Some examples of the unresolved and modeled flame surface density field are shown in figure 10. The model predicts well the locations of high contributions, in contrast with models based on the subgrid-scale velocity fluctuations (Nottin *et al*. 2000).

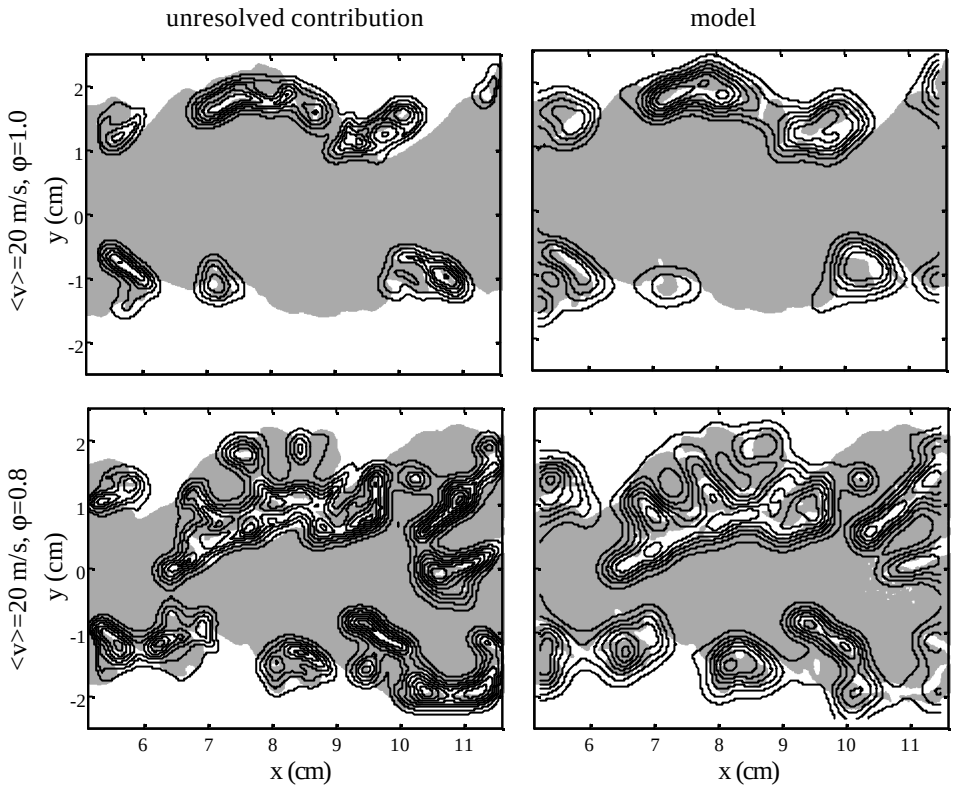

Figure 10. Iso-contours of the unresolved flame surface density (on the left) and the proposed model (on the right) with D=5 mm and k=0.6 for two different operating conditions. In gray is shown the binarized progress variable. Units are in cm.

CONCLUSION

An experimental method for the analysis of subgrid-scale combustion models is presented, based on OH-LIF images. Earlier comparisons with numerical simulations evidenced a deficiency of currently used models. A new model based on the curvature of the filtered progress variable is proposed. This model is able to predict correctly the locations of high unresolved contributions of the flame surface density. Analysis also shows that for limited values of the filter size, the model parameter is almost independent of the equivalence ratio. Further studies are necessary to determine the dependency of the parameter k on the velocity field and to test the applicability of the model in numerical simulations.

REFERENCES

Angelberger, C., Veynante, D., Egolfopoulos, F. and Poinsot, T. (1998). "Large eddy simulation of combustion instabilities in premixed flames", Proceedings of the Summer Program, Center for Turbulence Research, Stanford University – NASA Ames, pp.61-82.

Boger, M., Veynante, D., Boughanem, B. and Trouvé, A. (1998). "Direct numerical simulation analysis of flame surface density concept for large eddy simulation of turbulent premixed combustion", Twenty-Seventh Symposium (International) on Combustion, The Combustion Institute, pp.917-925.

Bourlioux, A., Moser, V. and Klein, R. (1996). "Large eddy simulations of turbulent premixed flames using a capturing/tracking hybrid approach", Sixth International Conference on Numerical Combustion, New Orleans, Louisiana.

Butler, T.D. and O'Rourke, P.J. (1977). "A numerical method for two-dimensional unsteady reactive flows", Sixteenth Symposium (International) on Combustion, The Combustion Institute, pp.1503-1515.

Colin, O., Ducros, F., Veynante, D. and Poinsot, T. (2000). “A thickened flame model for large eddy simulations of turbulent premixed combustion”, Phys. Fluids A, to be published.

Kerstein, A.R., Asherst, W. and Williams, F.A. (1988). “Field equation for interface propagation in an unsteady homogeneous flow field”, Phys. Rev. A, 37(7), pp.2728-2731.

Menon, S. (1996). “Large eddy simulations of combustion instabilities”, Sixth International Conference on Numerical Combustion, New Orleans, Louisiana.

Nottin, C., Knikker, R., Boger, M., Veynante, D. (2000). “Large eddy simulations of an acoustically excited turbulent premixed flame”, Twenty-Eight Symposium (International) on Combustion, The Combustion Institute, to be published.

Piana, J., Ducros, F. and Veynante, D. (1997). “Large eddy simulations of turbulent premixed flames based on the g-equation and a flame front wrinkling description”, Eleventh Symposium on Turbulent Shear Flows, Grenoble, France.